

Quantifying Impairment and Disease Severity Using AI Models Trained on Healthy Subjects

Boyang Yu¹, Aakash Kaku¹, Kangning Liu¹, Avinash Parnandi^{3,4}, Emily Fokas³, Anita Venkatesan³, Natasha Pandit³, Rajesh Ranganath^{1,2†}, Heidi Schambra^{3,4*†}
and Carlos Fernandez-Granda^{1,2*†}

¹Center for Data Science, New York University, NYU, 60 Fifth Ave, New York, 10011, New York, United States.

²Courant Institute of Mathematical Sciences, NYU, 251 Mercer St, New York, 10012, New York, United States.

³Department of Neurology, NYU Grossman School of Medicine, 550 1st Ave, New York, 10016, New York, United States.

⁴Department of Rehabilitation Medicine, NYU Grossman School of Medicine, 550 1st Ave, New York, 10016, New York, United States.

*Corresponding author(s). E-mail(s):

Heidi.Schambra@nyulangone.org; cfranda@cims.nyu.edu;

Contributing authors: boy.yu@nyu.edu; ark576@nyu.edu;

kl3141@nyu.edu; avinashparnandi@gmail.com;

emily.fokas@nyulangone.org; anita.venkatesan@nyulangone.org;

ngp238@nyu.edu; rajeshr@cims.nyu.edu;

†These authors contributed equally to this work.

Abstract

Automatic assessment of impairment and disease severity is a key challenge in data-driven medicine. We propose a novel framework to address this challenge, which leverages AI models trained exclusively on healthy individuals. The COncidence-Based chaRacterization of Anomalies (COBRA) score exploits the decrease in confidence of these models when presented with impaired or diseased patients to

quantify their deviation from the healthy population. We applied the COBRA score to address a key limitation of current clinical evaluation of upper-body impairment in stroke patients. The gold-standard Fugl-Meyer Assessment (FMA) requires in-person administration by a trained assessor for 30-45 minutes, which restricts monitoring frequency and precludes physicians from adapting rehabilitation protocols to the progress of each patient. The COBRA score, computed automatically in under one minute, is shown to be strongly correlated with the FMA on an independent test cohort for two different data modalities: wearable sensors ($\rho = \mathbf{0.845}$, 95% CI [0.743,0.908]) and video ($\rho = \mathbf{0.746}$, 95% C.I [0.594, 0.847]). To demonstrate the generalizability of the approach to other conditions, the COBRA score was also applied to quantify severity of knee osteoarthritis from magnetic-resonance imaging scans, again achieving significant correlation with an independent clinical assessment ($\rho = \mathbf{0.644}$, 95% C.I [0.585,0.696]).

Keywords: Deep learning, anomaly detection, impairment quantification, stroke rehabilitation, knee osteoarthritis

1 Introduction

In current clinical practice, assessment of impairment and disease severity typically relies on examinations by medical professionals [1, 2]. As a result, assessment is often qualitative and its frequency is constrained by clinician availability. Developing data-driven quantitative metrics of impairment and disease severity has the potential to enable continuous and objective monitoring of patient recovery or decline. Such monitoring would facilitate personalized treatment and administration of appropriate therapeutic interventions in telehealth and other remotely supervised contexts where ongoing access to clinicians is not readily available [3–5].

Artificial-intelligence (AI) models based on machine learning are a natural tool to perform data-driven patient assessment [6–19]. These models can be trained in a supervised fashion to estimate labels associated with patient data from large curated datasets of examples [11, 14, 20]. Unfortunately, it is often very challenging to assemble datasets containing an exhaustive representation of severity or impairment levels, which is necessary to ensure the accuracy of the AI models [21–26]. Moreover, supervised approaches require the existence of an objective quantitative metric that can be computed for every patient in the dataset, but such metrics do not exist for many medical conditions [27, 28].

To address these challenges, we consider the problem of performing automatic patient assessment using AI models trained *only on data from healthy subjects*. This is an anomaly detection problem, where the goal is to identify data points that are systematically different from a reference population [29]. Existing anomaly-detection methods for medical data are mostly based on

generative models [30, 31]. These models are designed to reconstruct high-dimensional data from a learned low-dimensional representation. Once trained, they are typically unable to accurately reconstruct data that are anomalous, due to their inconsistency with the training set. Consequently, the model reconstruction error tends to be higher for anomalies than for normal data, and can therefore be used as an anomaly-detection score. This approach has been applied to identify chronic brain infarcts [32], Alzheimer’s disease [33], microstructural abnormalities in diffusion MRI tractometry [34], and abnormalities of cosmetic breast reconstruction in cancer patients [35].

Anomaly detection based on generative models has an important disadvantage: it does not constrain the AI model to learn clinically relevant features. Consequently, the model reconstruction error may depend on properties of the data unrelated to the medical condition of interest. Here, we propose a novel anomaly-detection framework that is *tailored to a specific medical condition*. This is achieved by utilizing an AI model that predicts an attribute of the data, which is directly relevant to the condition (e.g. type of motion primitive performed by the stroke-impaired side, or tissue type for knee osteoarthritis). Crucially, the model is trained exclusively on healthy subjects, using annotated data describing the attribute. When the models are presented with data where the attribute is affected by the condition, we observe that the average model confidence tends to decrease proportionally to severity. This yields a quantitative patient-assessment metric, which we call the COncidence-Based chaRacterization of Anomalies (COBRA) score. Figure 1 provides a schematic description of the proposed framework.

The COBRA score is inspired by a technique proposed in [36], which identifies anomalous data points using the confidence of AI models. In this and subsequent works [37–41] anomalies were identified based on the loss of confidence of the AI models for a *single data point*. The effectiveness of this approach depends on the overlap in the distribution of confidences [42]. In our applications of interest, this is ineffective, as illustrated by Figure 2. When presented with multiple inputs from an impaired or diseased patient, AI models trained on healthy subjects tend to lose confidence *on average*, but the confidence for individual data points is very noisy and results in an unreliable metric. For this reason, the COBRA score is computed using multiple data points for each subject, corresponding to different motions in the application to stroke and to different pixels in the application to knee osteoarthritis. Aggregating the confidence associated with multiple data via averaging dramatically reduces the noise, resulting in a stable and accurate subject-level metric.

We apply the COBRA score to automatically evaluate the impairment level of stroke patients. Stroke commonly causes motor impairment in the upper extremity (UE), characterized by loss of strength, precise control, and intrusive muscle co-activation, which collectively interfere with normal function. Rehabilitation seeks to reduce motor impairment through the repeated practice of functional movements with the UE. In this process, it is crucial to monitor the impairment level of the patient. The gold-standard method of measuring

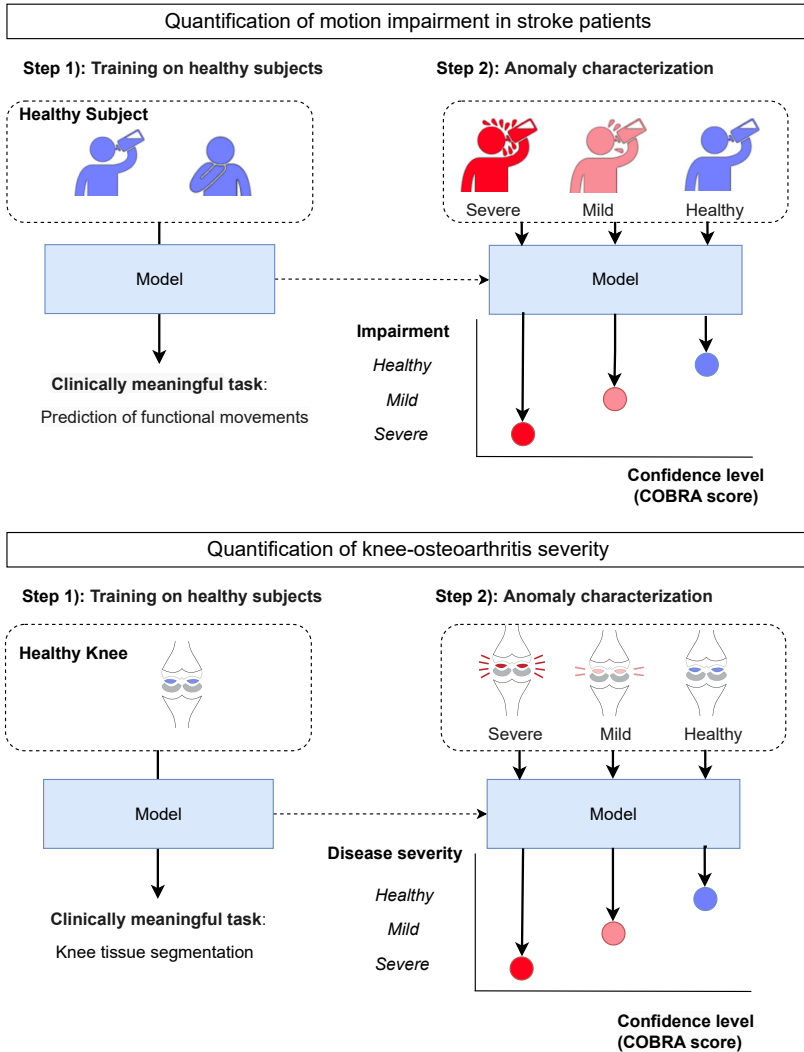


Fig. 1 The COntidence-Based chaRacterization of Anomalies (COBRA) score. In Step 1, an AI model is trained to perform a clinically meaningful task on data from healthy individuals. For impairment quantification in stroke patients, the task is prediction of functional primitive motions from videos or wearable-sensor data (top). For severity quantification of knee osteoarthritis, the task is segmentation of knee tissues from magnetic resonance imaging scans (bottom). In Step 2, the COBRA score is computed based on the confidence of the AI model when performing the task on patient data. Data from patients with higher degrees of impairment or severity differ more from the healthy population used for training, which results in decreased model confidence and hence a lower COBRA score.

motor impairment is the Fugl-Meyer Assessment (FMA) [2]. Unfortunately, it requires in-person administration by a trained assessor and is time-consuming

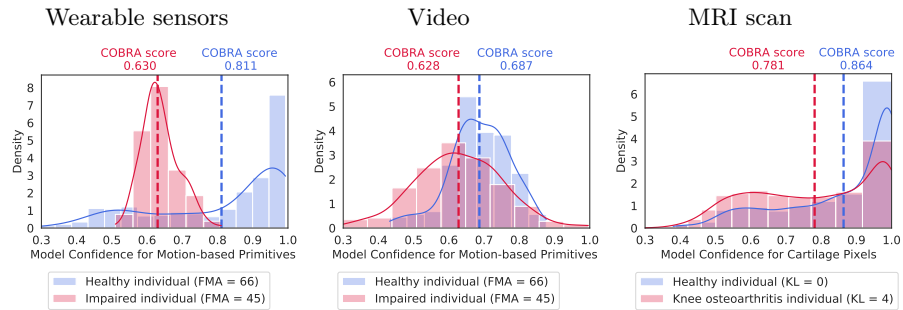


Fig. 2 Averaging model confidence yields a discriminative subject-level metric.

The plots show histograms and kernel density estimates of the confidence of a model trained on healthy subjects when presented with test data from an impaired or diseased patient (red), and from a held-out healthy individual (blue). The confidence distributions overlap, so individual values do not allow to discriminate between healthy and impaired individuals. In contrast, the average confidence is systematically higher for healthy subjects, and therefore provides a discriminative subject-level metric. The first and second plot correspond to wearable-sensor and video data associated with the same healthy and impaired individuals from the test cohort for quantification of stroke-induced impairment. The third plot corresponds to MRI scans from a healthy and diseased individual in the knee-osteoarthritis test cohort.

(30-45 minutes), which makes it impractical for frequent monitoring. Automatic assessment of motion impairment based on video or wearable-sensor data would address these limitations, facilitating actionable and granular tracking of motor recovery.

Motor impairment evaluation in stroke patients illustrates the difficulty of applying standard supervised AI methodology to patient assessment. An existing study shows the feasibility of the approach [43], but only includes 17 patients. Training a supervised model to predict impairment and rigorously evaluating its performance on held-out data requires a database of at least hundreds, and ideally thousands of patients, labeled with the corresponding impairment level. However, the largest such publicly available dataset consists of just 51 patients [44]. Here, we use this dataset as a held-out test set to evaluate the proposed framework.

In order to assess impairment in stroke patients using the COBRA score, we trained AI models to predict classes of UE motion, known as functional primitives, performed by a group of healthy individuals. We used upper-body motion data obtained from videos and wearable sensors. The model was then applied to data from a test cohort of stroke patients and held-out healthy subjects performing nine different stroke rehabilitation activities. The confidence of the motion predictions for each test subject was averaged to compute the corresponding COBRA score. As reported in Section 2.1, for both data modalities the COBRA score is correlated with the Fugl-Meyer Assessment of the patients, obtained in person by trained experts. This greatly expands on our preliminary findings, which used a similar approach with wearable-sensor data from a single rehabilitation activity [45].

Table 1 Demographic and clinical characteristics of the training and test cohorts for the application to quantification of motion impairment in stroke patients. The mean \pm standard deviation is reported for age, Fugl-Meyer assessment and time since stroke.

	Training	Testing
Number of subjects	25	55
Trials	1265	2183
Age	62.4 \pm 13.1	57.7 \pm 14.0
Sex	13 male, 12 female	25 male, 30 female
Race ¹	10 W, 12 B, 0 A, 1 AI, 2 O	24 W, 14 B, 9 A, 0 AI, 8 O
Paretic Side	n/a	28 left, 23 right, 4 n/a
Fugl-Meyer Assessment	66	43.5 \pm 16.2
Impairment level ²	25 healthy	4 healthy, 20 mild, 23 moderate, 8 severe
Time since stroke	n/a	5.4 \pm 6.1 (for stroke patients)

¹Race: White (W), Black (B), Asian (A), American Indian (AI), Other (O)

²Based on FMA: 0-25 is severe, 26-52 moderate, 53-65 mild, and 66 healthy.

To demonstrate the general applicability of the COBRA framework, we show that it can be used to evaluate severity of knee osteoarthritis from magnetic resonance imaging (MRI) scans. Knee osteoarthritis is a musculoskeletal disorder characterized by a progressive loss of knee cartilage. To quantify severity, we trained an AI model to perform segmentation of different knee tissues (including cartilage) on MRIs of healthy knees. We then applied the model to knee MRIs from a test cohort of diseased patients and held-out healthy subjects. The confidence of the tissue predictions for each test subject was averaged to compute the corresponding COBRA score. As reported in Section 2.2, the resulting COBRA score is again highly correlated with an independent assessment of disease severity (in this case, the Kellgren-Lawrence grade).

2 Results

2.1 Quantification of Impairment in Stroke Patients

Data. The application of the COBRA score to the impairment quantification in stroke patients was carried out using the publicly available StrokeRehab dataset [44]. StrokeRehab contains video and wearable-sensor data from a cohort of 29 healthy individuals and 51 stroke patients performing multiple trials of nine rehabilitation activities (described in Tables A1 and A2). The impairment level of each patient was quantified via the Fugl-Meyer assessment (FMA) [2]. The FMA score is a number between 0 (maximum impairment) and 66 (healthy) equal to the sum of itemized scores (each from 0 to 2) for 33 upper body mobility assessments carried out in-clinic by a trained expert. The wearable-sensor and video data are labeled to indicate what functional primitive is being performed by the paretic arm over time: reach (UE motion to make contact with a target object), reposition (UE motion to move into proximity of a target object), transport (UE motion to convey a target object in space), stabilization (minimal UE motion to hold a target object still), and idle (minimal UE motion to stand at the ready near a target object).

Computation of COBRA score. AI models were trained to predict the functional primitives performed by a training cohort consisting of 25 of the 29 healthy individuals (selected at random). The model input was either wearable sensor or video data. Detailed descriptions of these models are provided in Section 4.2. The models were applied to a test cohort consisting of the remaining 4 healthy individuals and the 51 stroke patients. Demographic and clinical information about the training and test cohorts is provided in Table 1. The COBRA score was calculated as the average of the model confidence for data points identified by the models as corresponding to functional primitives that involve motion (*transport*, *reposition*, and *reach*), as described in Section 4.2.

Evaluation. The COBRA score was evaluated by computing its Pearson correlation coefficient with the Fugl-Meyer Assessment (FMA) score [2] on the test cohort of 51 stroke patients and 4 healthy individuals (n=55). The correlation coefficient is 0.814 (95% CI [0.700,0.888]) for the wearable-sensor data and 0.736 (95% CI [0.584, 0.838]) for the video data. Figure 3 (a) shows scatterplots of the COBRA and FMA scores. For both data modalities, the COBRA score has a strong, statistically significant correlation with the in-clinic assessment.

Figure 4 reports the correlation coefficients between the FMA score and the COBRA score computed using subsets of the data corresponding to individual rehabilitation activities (see Tables A1 and A2 for a detailed description of the activities). Scatterplots of the FMA and COBRA scores for each activity are provided in Figures B2 and B3. For both data modalities, the correlation is higher for more structured activities (moving objects to targets on a table-top or shelf, donning glasses) and is lower for more complex activities (hair-combing, face-washing, teeth-brushing, feeding), which tend to involve more heterogeneous motions across individuals. The correlation coefficient with the FMA score is lower for the COBRA score computed from individual activities than for the COBRA score that aggregates all activities. The only exception is the table-top task, which is the most regular and structured activity. The corresponding COBRA score computed from wearable-sensor data is very high (0.849, 95% CI [0.752, 0.910]), which suggests that it may be possible to obtain accurate impairment assessment from a reduced number of data using activities that are highly structured.

An important consideration when applying the proposed framework is that extraneous factors may produce a spurious decrease in the confidence of the AI model. Figure 5 shows that this occurs for the table-top activity, which was carried out with light-colored and dark-colored objects by different subjects. Dark objects are much more difficult to detect in videos, which produces a systematic loss of confidence in the video-based AI model that translates to lower COBRA scores. This explains why the correlation between the FMA score and the COBRA score is lower for the table-top video data than for the table-top wearable-sensor data, which is unaffected by this confounding factor. As depicted in Figure 5, we can correct for the confounding factor by stratifying the subjects according to the object color. This increases the COBRA score from 0.615 (95% CI [0.411, 0.760]) to 0.679 (95% CI [0.294, 0.874]) for dark

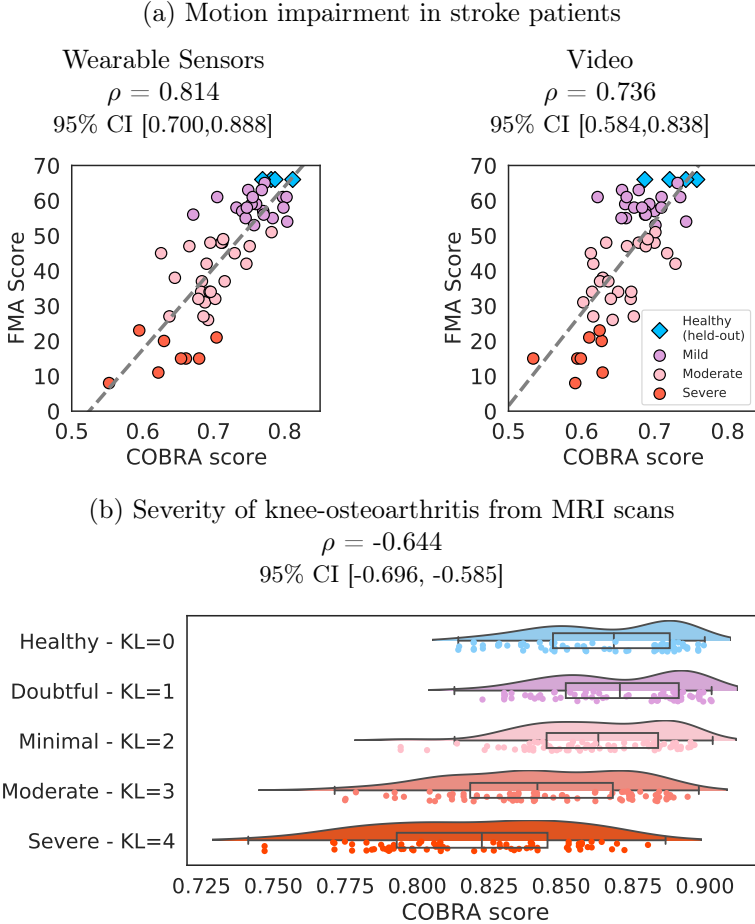


Fig. 3 Correlation between the COBRA score and clinical assessment. The top row shows scatterplots of the Fugl-Meyer assessment (FMA) score, based on in-person examination by an expert, and the proposed data-driven COBRA score computed from wearable-sensor (left) and video (right) data. The correlation coefficient ρ between the two scores is high, particularly for the wearable-sensor data. The second row shows a scatterplot and density plots of COBRA scores computed from magnetic-resonance imaging (MRI) knee scans of patients with different Kellgren-Lawrence (KL) grades. The KL grade and the COBRA score exhibit significant inverse correlation.

objects and 0.756 (95% CI [0.553, 0.874]) for light objects. For comparison, the correlation of the video-based COBRA score computed from all activities is 0.736 (95% CI [0.584,0.838]). Figure B4 shows that image quality can also act as a confounding factor: blurring the video images results in a systematic decrease of the COBRA score, which can also be corrected via stratification.

The COBRA score is computed as an average of the AI-model confidence for data points identified by the model as corresponding to functional actions that involve motion (*reach*, *reposition*, *transport*), as opposed to functional

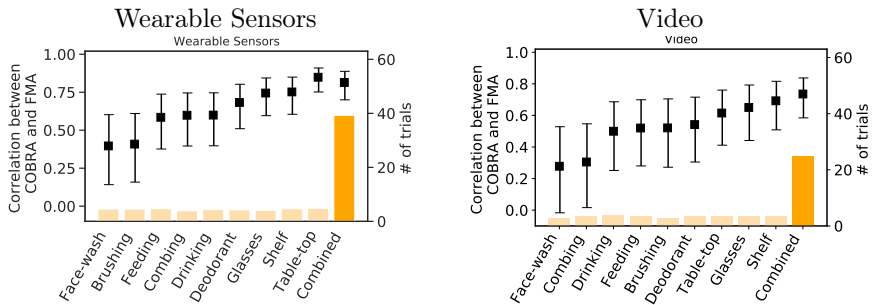


Fig. 4 Impairment quantification from individual rehabilitation activities. The graph shows the correlation coefficient (indicated by black markers with 95% confidence intervals) between the Fugl-Meyer score of stroke patients, and the COBRA score computed from single activities using wearable-sensor (left) or video (right) data. The number of trials available for each activity are indicated by the yellow bars. Simple, more structured activities (Glasses, Shelf, Table-top) have higher correlation than more complicated activities (Face-wash, Feeding, Combing) for both data modalities.

Table 2 Demographic and clinical characteristics of study participants for the application to quantification of knee-osteoarthritis severity. The mean \pm standard deviation is reported for age.

	Training	Testing
Number of individuals	44	435
Age	59.2 \pm 8.2	62.0 \pm 9.4
Sex	20 male, 24 female	228 male, 207 female
Race ¹	36 W, 7 B, 1 O	339 W, 81 B, 5 A, 10 O
Kellgren-Lawrence grades	44 healthy (KL=0)	57 healthy (KL=0)
		58 doubtful (KL=1)
		109 minimal (KL=2)
		138 moderate (KL=3)
		73 severe (KL=4)

¹Race: White (W), Black (B), Asian (A), Other (O)

actions that do not (*rest, stabilize*). These data can be considered as *clinically relevant* to impairment quantification associated with motion. Figure 6 shows that the correlation coefficient between the FMA score and a COBRA score computed from data points identified as non-motion functional actions is low (in fact, for the video data it is not even statistically significant). It also shows that a COBRA score computed from all actions has a lower correlation with the FMA score than the proposed motion-based COBRA score for both data modalities.

2.2 Quantification of Knee-Osteoarthritis Severity

Data. The application of the COBRA score to the quantification of knee-osteoarthritis (OA) severity was carried out using the publicly available OAI-ZIB dataset [46]. This dataset provides 3D MRI scans of 101 healthy right knees

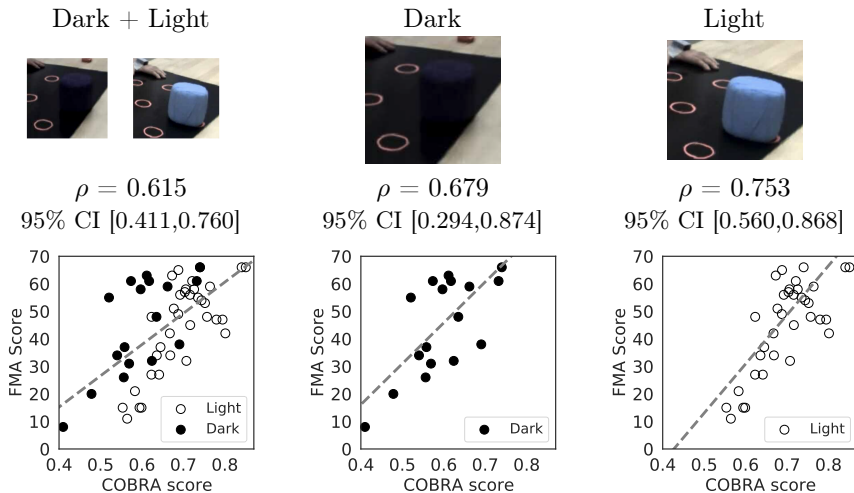


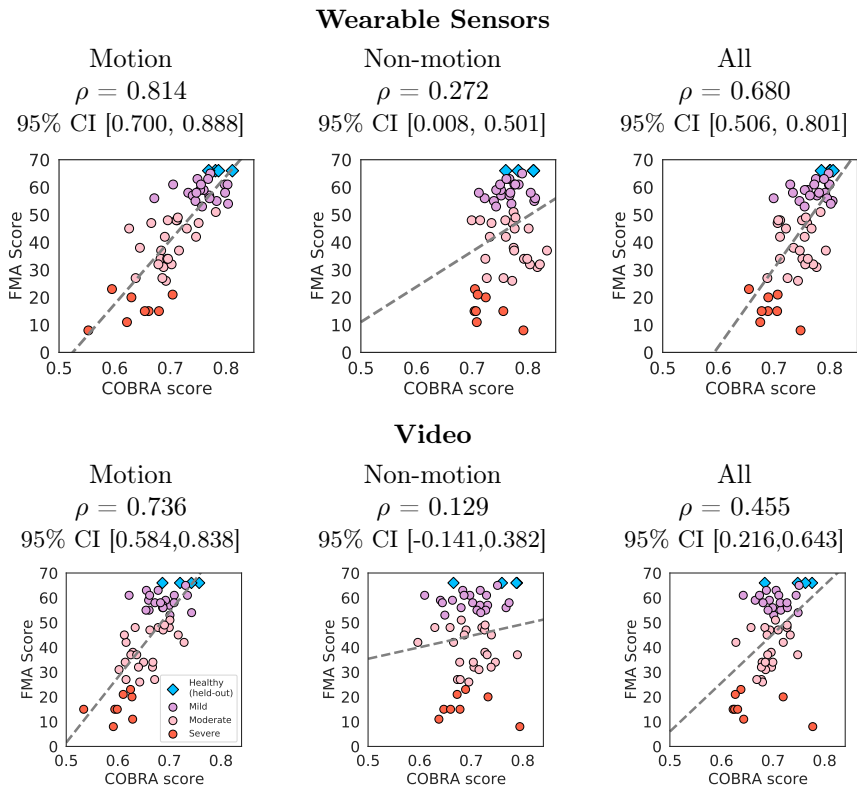
Fig. 5 Object color as a confounding factor for the video-based COBRA score and correction via stratification. The table-top rehabilitation activity in the stroke impairment quantification task involves dark and light-colored objects (top row). The bottom left scatterplot shows the COBRA score computed only using video data from this activity and the corresponding Fugl-Meyer assessment (FMA) score. The dark objects are difficult to detect, which results in a systematic loss of confidence in the video-based AI model, and hence lower COBRA scores (independently from the FMA score). The bottom middle and right scatterplots show that stratifying according to object color corrects for the confounding factor, improving the correlation coefficient ρ between the COBRA and FMA scores.

and 378 right knees affected by knee osteoarthritis, a long-term degenerative joint condition. Each knee is labeled with the corresponding Kellgren-Lawrence (KL) grade [47], retrieved from the NIH Osteoarthritis Initiative collection [48]. The KL grade quantifies OA severity on a scale from 0 (healthy) to 4 (severe), as illustrated in Figure A1. Each voxel in the MRI scans is labeled to indicate the corresponding tissue (*tibia bone*, *tibia cartilage*, *femur bone*, *femur cartilage* or *background*).

Computation of COBRA Score. An AI segmentation model was trained to predict the tissue at each voxel using a training cohort of 44 healthy individuals (selected at random). A detailed description of this model is provided in Section 4.3. The model was applied to a test cohort consisting of the remaining 57 healthy individuals and the 378 patients with knee OA. Demographic and clinical information about the training and test cohorts is provided in Table 2. The COBRA score was calculated as the average of the model confidence for data points identified by the models as corresponding to cartilage tissue (*tibia cartilage* and *femur cartilage*), as described in Section 4.3.

Evaluation. The COBRA score was evaluated by computing its Pearson correlation coefficient with the Kellgren-Lawrence (KL) grading scores [47] on the test cohort of 378 patients with knee OA and 57 healthy subjects ($n=435$), which equals -0.644 (95% CI $[-0.696, -0.585]$). There is therefore a significant

(a) Motion impairment in stroke patients



(b) Severity of knee-osteoarthritis from MRI scans

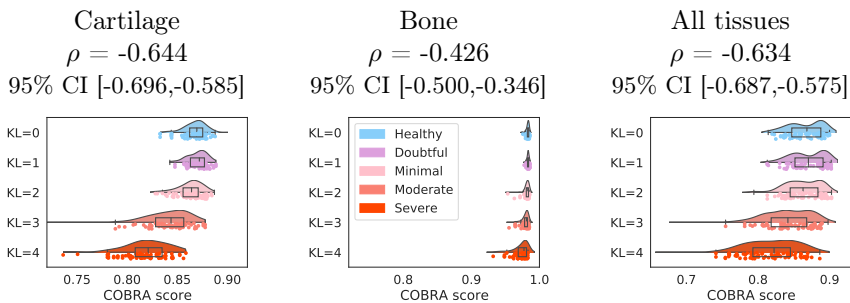


Fig. 6 The COBRA score exploits clinically-relevant structure. The left column shows scatterplots of clinical assessments (Fugl-Meyer assessment and Kellgren-Lawrence grade for the stroke and knee-osteoarthritis applications respectively) and the proposed COBRA score, computed from data identified as clinically relevant (motion actions for stroke, cartilage tissue for knee osteoarthritis). The middle and right column shows scatterplots for COBRA scores computed from the remaining data, and from all the data respectively. Using clinically relevant data consistently achieves a higher correlation with the clinical assessments.

inverse correlation between the scores, indicating that the COBRA score quantifies knee OA severity. Figure 3(b) shows scatterplots and density plots of the COBRA scores corresponding to different KL grades.

The COBRA score is computed as an average of the AI-model confidence for voxels identified by the model as corresponding to cartilage, as opposed to bone tissue. These data can be considered as *clinically relevant* because knee OA produces gradual degradation of articular cartilage (bone alterations and osteophyte formation may also occur, but are less frequent) [49, 50]. Figure 6 shows that the magnitude of the correlation coefficient between the KL score and a COBRA score is significantly lower than for cartilage. The magnitude of the correlation coefficient for the COBRA score computed from all voxels is only slightly lower than that of the proposed motion-based COBRA score, indicating that including bone is not very detrimental.

3 Discussion

In this work we introduce the COBRA score, a data-driven anomaly-detection framework for automatic quantification of impairment and disease severity. We show its utility for clinically relevant quantification in two different medical conditions (stroke and knee osteoarthritis) and in three different data modalities (wearable sensors, video and MRI). The framework is suitable for applications where it is challenging to gather large-scale databases of patients with different degrees of impairment or severity, as it only requires data from a healthy cohort of moderate size.

From a methodological perspective, our results suggest that fine-grained annotations describing clinically relevant attributes can be useful *even if they are only available for healthy subjects*. We hypothesize that AI models trained with such annotations can be leveraged in different ways beyond the proposed approach. To illustrate this, an alternative anomaly-detection procedure that does not utilize model confidence is included in Section C.

Our study identifies a key consideration when applying the proposed framework: confounding factors unrelated to the medical condition of interest (e.g. object color or blurriness in a video) can influence the confidence of the AI models, and therefore distort the COBRA score. This is an instance of a general challenge inherent to the use of deep neural networks: these models are so flexible that they can easily learn spurious structure in high-dimensional data [42, 51]. Our results suggest that the influence of confounding factors can be mitigated by gathering a sufficiently diverse training set (e.g. including diverse rehabilitation activities in the case of stroke-induced impairment) and that it is possible to explicitly correct for known confounding factors via stratification. Nevertheless, automatic identification and control of confounders is an important topic for future research.

4 Methods

In this section we describe a general framework to estimate impairment and disease severity using AI models trained only on data from healthy subjects. We frame this as an anomaly detection and quantification problem, where the goal is to identify subjects that deviate from the healthy population, and to quantify the extent of this deviation. Section 4.1 describes the proposed framework, and Sections 4.2 and 4.3 describe how we apply it to quantify impairment in stroke patients and severity of knee osteoarthritis respectively.

4.1 Confidence-based Characterization of Anomalies

The proposed COncidence-Based chaRacterization of Anomalies (COBRA) framework utilizes a model trained to perform an AI task only on healthy patients. Intuitively, if the model has low confidence when performing the task on a new subject, this indicates that the subject deviates from the healthy population. In order to ensure that this deviation is due to a certain type of impairment or disease, it is crucial to choose an appropriate AI task. For quantification of stroke-induced impairment, we predict the functional actions carried out by the subject from wearable sensor or video data. For the application to knee osteoarthritis, we predict the tissue present in each voxel of a 3D MRI scan.

Let us assume that we have access to a training cohort of N_{train} healthy subjects, and that each of them is associated with a set of annotated data relevant to the medical condition of interest:

$$\mathcal{T}_i := \left\{ \left(x_1^{[i]}, y_1^{[i]} \right), \dots, \left(x_{M_i}^{[i]}, y_{M_i}^{[i]} \right) \right\}, \quad 1 \leq i \leq N_{\text{train}}. \quad (1)$$

Here $x_j^{[i]} \in \mathbb{R}^L$ denotes the j th data point associated with the i th subject, and M_i is the number of data available for that subject. The label $y_j^{[i]} \in \{1, \dots, K\}$ assigns $x_j^{[i]}$ to one of K predefined classes. For the stroke application, the label encodes the functional action carried out by the subject at a certain time. The corresponding data point is a segment of wearable-sensor or video data. For the knee-osteoarthritis application, the label encodes the type of tissue at a certain position in the knee, and the corresponding data are surrounding MRI voxels.

The training dataset

$$\mathcal{S}_{\text{train}} := \{ \mathcal{T}_1, \dots, \mathcal{T}_{N_{\text{train}}} \} \quad (2)$$

is used to train an AI model $f : \mathbb{R}^L \rightarrow [0, 1]^K$ to predict the labels from the data. The input to the model is an L -dimensional data point and the output is a K dimensional vector

$$p_j^{[i]} := f(x_j^{[i]}), \quad 1 \leq i \leq N_{\text{train}}, \quad 1 \leq j \leq M_i, \quad (3)$$

where the k th entry is an estimate of the probability that the data point belongs to the k th class. In our applications of interest, the models are deep neural networks, described in detail in Sections 4.2 and 4.3. Crucially, if the dataset associated with each subject is large, then the total number of training examples

$$M_{\text{train}} := \sum_{i=1}^{N_{\text{train}}} M_i \quad (4)$$

is orders of magnitude larger than the number of training subjects N_{train} . This enables us to train deep-learning models using relatively small training cohorts.

Let $X_{\text{test}} := \{x_1^{\text{test}}, \dots, x_{M_{\text{test}}}^{\text{test}}\}$ denote a dataset associated with a test subject. We can obtain probabilities corresponding to each test data point by applying the trained AI model,

$$p_j^{\text{test}} := f(x_j^{\text{test}}), \quad 1 \leq j \leq M_{\text{test}}. \quad (5)$$

This yields a prediction of the class associated with each example

$$\hat{y}_j^{\text{test}} := \arg \max_{1 \leq k \leq K} p_j^{\text{test}}[k], \quad (6)$$

where $p_j^{\text{test}}[k]$ denotes the k th entry of p_j^{test} . The estimated probability that the data point belongs to the predicted class is commonly known as the *confidence* of the model (see e.g. [52]),

$$c_j^{\text{test}} := \max_{1 \leq k \leq K} p_j^{\text{test}}[k], \quad (7)$$

because it can be interpreted as an estimate of the probability that the model prediction is correct.

Several existing works propose to use confidence values to perform anomaly detection [36–41]. Intuitively, if a model is well trained (and there is no inherent uncertainty in the training labels [53]), it should be able to confidently classify new examples. Therefore low model confidence is evidence that the data point may be anomalous, in the sense that it deviates from the training distribution. Our proposed framework builds upon this idea, incorporating two novel elements. First, multiple data points are aggregated to perform subject-level anomaly detection. As illustrated by Figure 2, this is critical to achieve accurate anomaly detection in our applications of interest, because the individual confidences are very noisy. Second, we determine which of the classes are most clinically-relevant, and restrict our attention to data points predicted to belong to those classes. As reported in Figure 6, for the stroke application this provides a substantial improvement over using all the data.

Let $\mathcal{R} \subseteq \{1, \dots, K\}$ denote the subset of clinically-relevant classes, and

$$\mathcal{J}_{\text{relevant}} := \{j : \hat{y}_j^{\text{test}} \in \mathcal{R}\} \quad (8)$$

the subset of test data predicted to belong to those classes. We define the COBRA score as the arithmetic average of the confidences associated with the data in $\mathcal{J}_{\text{relevant}}$,

$$\text{COBRA}(X_{\text{test}}) := \frac{1}{|\mathcal{J}_{\text{relevant}}|} \sum_{j \in \mathcal{J}_{\text{relevant}}} c_j^{\text{test}}. \quad (9)$$

The lower the COBRA score, the less confident the AI model is on average when performing the task on the test subject, which indicates a greater degree of impairment or disease.

4.2 Estimation of Stroke-Related Motor Impairment

In order to apply the COBRA framework to automatic impairment quantification in stroke patients, we propose to utilize auxiliary AI models trained to predict the functional primitive carried out by the subjects' paretic upper extremity (UE) while performing rehabilitation activities. The $K := 5$ primitive classes are *reach*, *reposition*, *transport*, *stabilize*, and *rest*. UE motor impairment affects the three functional primitives involving motion

$$\mathcal{R} := \{ \textit{transport}, \textit{reposition}, \textit{reach} \}, \quad (10)$$

rendering them systematically different to those of healthy individuals. Our hypothesis is that this causes AI models trained on healthy subjects to lose confidence when they are applied to stroke patients, and that the loss of confidence is indicative of the degree of impairment. In the remainder of this section we describe the AI models that we use to test this hypothesis for two different data modalities, wearable sensors and video.

4.2.1 Wearable sensors

The wearable-sensor data is a 77-dimensional time series, recorded at 100 Hz using nine inertial measurement units (IMUs) attached to the upper body [44]. The data correspond to kinematic features of 3D linear accelerations, 3D quaternions, joint angles from the upper body, and a binary value that indicates the side (left or right) performing the motion. In order to identify functional primitives from these data, we utilized a Multi-Stage Temporal Convolutional Network (MS-TCN) [54].

MS-TCN is a state-of-the-art deep-learning model for action segmentation consisting of four convolutional stages, each composed of 10 layers of dilated residual convolutions with 64 output channels. A softmax layer at the end of the network produces the final output, which is a 5-dimensional vector indicating the probability that each entry in the time series corresponds to each functional primitive. The model was trained on the healthy training cohort using the weighted cross-entropy loss function proposed in [55]. This cost function was minimized for 50 epochs using the Adam optimizer [56] with a learning

rate of $5 \cdot 10^{-3}$ (selected via cross-validation). The accuracy and precision of the resulting model are shown in Appendix B4.

4.2.2 Video

The video data were acquired with two high-speed (60 Hz), high-definition (1088×704 resolution) cameras (Ninox, Noraxon) positioned orthogonally <2 m from the subject. The cameras have a focal length of f4.0 mm and a large viewing window (length: 2.5 m, width: 2.5 m). The videos were then downsampled to a resolution of 256×256 to enable efficient processing. To perform functional primitive identification from these data, we utilized the X3D model [57], a 3D convolutional neural network designed for primitive classification from video data. The model was pretrained on the Kinetic dataset [58], where the labels are high-level activities such as running, climbing, sitting, etc.

After pretraining, the X3D model was fine-tuned to perform classification of functional primitives on the rehabilitation activities performed by the healthy training cohort. The input to the model are video segments with duration two seconds, and the output is the estimated probability that the central frame corresponds to each of the five functional primitives. Model fine-tuning was carried out by minimizing the cross entropy between these probabilities and the functional primitive labels via stochastic gradient descent with a base learning rate of 0.01 and a cosine learning rate policy. The accuracy and precision of the resulting model on held-out subjects are reported in Section B.1.

4.3 Estimation of Knee-Osteoarthritis Severity

In order to apply the COBRA framework to automatic quantification of knee-osteoarthritis severity we propose to utilize an auxiliary AI model trained to predict the type of tissue in each voxel of a 3D MRI scan. The $K := 5$ classes for this classification problem are *femur bone*, *femur cartilage*, *tibia bone*, *tibia cartilage* and *background* (indicating absence of tissue). Knee osteoarthritis deforms cartilage structure, so the clinically-relevant labels are chosen to be

$$\mathcal{R} := \{\textit{femur cartilage}, \textit{tibia cartilage}\}. \quad (11)$$

Our hypothesis is that the systematic difference in cartilage structure causes AI models trained on healthy knees to lose confidence when applied to diseased knees, and that the loss of confidence is indicative of disease severity.

In order to predict tissue type we applied a Multi-Planar U-Net [59]. The model processes the input 3D MRI scan from different views using a version of the 2D U-Net architecture [60]. The output from the different views are then averaged to produce a probability estimate at each 3D voxel. During training, random elastic deformations (RED) are randomly applied to a third of the images in each batch to improve generalization [59].

The model was trained by minimizing the cross entropy loss between the estimated probabilities and the 3D voxel-wise labels corresponding to 37 of

the 44 healthy individuals in the training cohort. The remaining 7 individuals were used as a validation set. In the cost function, images augmented via RED were downweighted by a factor of 1/3. The Adam optimizer was used for minimization, with an initial learning rate of $5 \cdot 10^{-5}$ that was reduced by 10% after two consecutive epochs without improvement in the validation Dice score. A criterion based on the validation Dice score (excluding background) was used to perform early stopping. Additional hyperparameters are listed in Table S.1 of [59]. The accuracy and precision of the resulting model are reported in Section B7.

Declarations

- Authors' contributions: H.S. and C.F.G. conceived the project. B.Y., A.K., K.L. and A.P. designed, implemented and evaluated the methodology with guidance from R.R., H.S. and C.F.G. A.P., E.F, A.V., and N.P. quality-checked the data and their annotations. B.Y., A.K., K.L., A.P., R.R., H.S. and C.F.G. wrote the paper with input from all authors.
- Competing interests The authors declare no competing interests.
- Acknowledgements This work was supported by NIH grant R01 LM013316, Alzheimer's Association grant AARG-NTF-21-848627, and NSF grant NRT-1922658.
- Data availability: Data to reproduce all results are available at <https://github.com/fishneck/COBRA/tree/main/data>.
- Code availability: Code to reproduce all results is available at <https://github.com/fishneck/COBRA>.

References

- [1] Medsger, T.A., Bombardieri, S., Czirják, L., Scorza, R., Rossa, A.D., Ben-civelli, W.: Assessment of disease severity and prognosis. *Clinical and experimental rheumatology* **21**(3; SUPP/29), 42–46 (2003)
- [2] Fugl-Meyer, A.R., Jääskö, L., Leyman, I., Olsson, S., Steglind, S.: A method for evaluation of physical performance. *Scand. J. Rehabil. Med* **7**(1), 13–31 (1975)
- [3] Raman, G., Ashraf, B., Demir, Y.K., Kershaw, C.D., Cheruku, S., Atis, M., Atis, A., Atar, M., Chen, W., Ibrahim, I., *et al.*: Machine learning prediction for covid-19 disease severity at hospital admission. *BMC Medical Informatics and Decision Making* **23**(1), 1–6 (2023)
- [4] Hwangbo, S., Kim, Y., Lee, C., Lee, S., Oh, B., Moon, M.K., Kim, S.-W., Park, T.: Machine learning models to predict the maximum severity of covid-19 based on initial hospitalization record. *Frontiers in Public Health* **10** (2022)

- [5] Shamout, F.E., Shen, Y., Wu, N., Kaku, A., Park, J., Makino, T., Jas-trzębski, S., Witowski, J., Wang, D., Zhang, B., *et al.*: An artificial intelligence system for predicting the deterioration of covid-19 patients in the emergency department. *NPJ digital medicine* **4**(1), 80 (2021)
- [6] Cottrell, M.A., Galea, O.A., O’Leary, S.P., Hill, A.J., Russell, T.G.: Real-time telerehabilitation for the treatment of musculoskeletal conditions is effective and comparable to standard practice: a systematic review and meta-analysis. *Clinical rehabilitation* **31**(5), 625–638 (2017)
- [7] Laver, K.E., Adey-Wakeling, Z., Crotty, M., Lannin, N.A., George, S., Sherrington, C.: Telerehabilitation services for stroke. *Cochrane Database of Systematic Reviews* (1) (2020)
- [8] Hamet, P., Tremblay, J.: Artificial intelligence in medicine. *Metabolism* **69**, 36–40 (2017)
- [9] Palanica, A., Docktor, M.J., Lieberman, M., Fossat, Y.: The need for artificial intelligence in digital therapeutics. *Digital Biomarkers* **4**(1), 21–25 (2020)
- [10] Ting, D.S., Lin, H., Ruamviboonsuk, P., Wong, T.Y., Sim, D.A.: Artificial intelligence, the internet of things, and virtual clinics: ophthalmology at the digital translation forefront. *The Lancet Digital Health* **2**(1), 8–9 (2020)
- [11] Topol, E.J.: High-performance medicine: the convergence of human and artificial intelligence. *Nature medicine* **25**(1), 44–56 (2019)
- [12] Barnes, R., Zvarikova, K.: Artificial intelligence-enabled wearable medical devices, clinical and diagnostic decision support systems, and internet of things-based healthcare applications in covid-19 prevention, screening, and treatment. *American Journal of Medical Research* **8**(2), 9–22 (2021)
- [13] Jeddi, Z., Bohr, A.: Remote patient monitoring using artificial intelligence. In: *Artificial Intelligence in Healthcare*, pp. 203–234. Elsevier, ??? (2020)
- [14] Shaik, T., Tao, X., Higgins, N., Li, L., Gururajan, R., Zhou, X., Acharya, U.R.: Remote patient monitoring using artificial intelligence: Current state, applications, and challenges. *Wiley Interdisciplinary Reviews: Data Mining and Knowledge Discovery* **13**(2), 1485 (2023)
- [15] Sawyer, J., *et al.*: Wearable internet of medical things sensor devices, artificial intelligence-driven smart healthcare services, and personalized clinical care in covid-19 telemedicine. *American Journal of Medical Research* **7**(2), 71–77 (2020)

- [16] Akbilgic, O., Obi, Y., Potukuchi, P.K., Karabayir, I., Nguyen, D.V., Soohoo, M., Streja, E., Molnar, M.Z., Rhee, C.M., Kalantar-Zadeh, K., *et al.*: Machine learning to identify dialysis patients at high death risk. *Kidney international reports* **4**(9), 1219–1229 (2019)
- [17] Chen, F., Kantagowit, P., Nopsopon, T., Chuklin, A., Pongpirul, K.: Prediction and diagnosis of chronic kidney disease development and progression using machine-learning: Protocol for a systematic review and meta-analysis of reporting standards and model performance. *Plos one* **18**(2), 0278729 (2023)
- [18] Babenko, B., Mitani, A., Traynis, I., Kitade, N., Singh, P., Maa, A.Y., Cuadros, J., Corrado, G.S., Peng, L., Webster, D.R., *et al.*: Detection of signs of disease in external photographs of the eyes via deep learning. *Nature Biomedical Engineering*, 1–14 (2022)
- [19] Shen, Y., Wu, N., Phang, J., Park, J., Liu, K., Tyagi, S., Heacock, L., Kim, S.G., Moy, L., Cho, K., *et al.*: An interpretable classifier for high-resolution breast cancer screening images utilizing weakly supervised localization. *Medical image analysis* **68**, 101908 (2021)
- [20] Beam, A.L., Kohane, I.S.: Big data and machine learning in health care. *Jama* **319**(13), 1317–1318 (2018)
- [21] Ching, T., Himmelstein, D.S., Beaulieu-Jones, B.K., Kalinin, A.A., Do, B.T., Way, G.P., Ferrero, E., Agapow, P.-M., Zietz, M., Hoffman, M.M., *et al.*: Opportunities and obstacles for deep learning in biology and medicine. *Journal of The Royal Society Interface* **15**(141), 20170387 (2018)
- [22] Norori, N., Hu, Q., Aellen, F.M., Faraci, F.D., Tzovara, A.: Addressing bias in big data and ai for health care: A call for open science. *Patterns* **2**(10), 100347 (2021)
- [23] Van Horn, J.D., Grethe, J.S., Kostelec, P., Woodward, J.B., Aslam, J.A., Rus, D., Rockmore, D., Gazzaniga, M.S.: The functional magnetic resonance imaging data center (fmridc): the challenges and rewards of large-scale databasing of neuroimaging studies. *Philosophical Transactions of the Royal Society of London. Series B: Biological Sciences* **356**(1412), 1323–1339 (2001)
- [24] Langs, G., Hanbury, A., Menze, B., Müller, H.: Visceral: towards large data in medical imaging—challenges and directions. In: *Medical Content-Based Retrieval for Clinical Decision Support: Third MICCAI International Workshop, MCBR-CDS 2012, Nice, France, October 1, 2012, Revised Selected Papers 3*, pp. 92–98 (2013). Springer

- [25] Oakden-Rayner, L., Dunnmon, J., Carneiro, G., Ré, C.: Hidden stratification causes clinically meaningful failures in machine learning for medical imaging. In: Proceedings of the ACM Conference on Health, Inference, and Learning, pp. 151–159 (2020)
- [26] Roy, S., Meena, T., Lim, S.-J.: Demystifying supervised learning in health-care 4.0: A new reality of transforming diagnostic medicine. *Diagnostics* **12**(10), 2549 (2022)
- [27] Jarrett, D., Stride, E., Vallis, K., Gooding, M.J.: Applications and limitations of machine learning in radiation oncology. *The British journal of radiology* **92**(1100), 20190001 (2019)
- [28] Varoquaux, G., Cheplygina, V.: Machine learning for medical imaging: methodological failures and recommendations for the future. *NPJ digital medicine* **5**(1), 48 (2022)
- [29] Chandola, V., Banerjee, A., Kumar, V.: Anomaly detection: A survey. *ACM computing surveys (CSUR)* **41**(3), 1–58 (2009)
- [30] Akcay, S., Atapour-Abarghouei, A., Breckon, T.P.: Ganomaly: Semi-supervised anomaly detection via adversarial training. In: *Computer Vision—ACCV 2018: 14th Asian Conference on Computer Vision, Perth, Australia, December 2–6, 2018, Revised Selected Papers, Part III 14*, pp. 622–637 (2019). Springer
- [31] Deecke, L., Vandermeulen, R., Ruff, L., Mandt, S., Kloft, M.: Image anomaly detection with generative adversarial networks. In: *Machine Learning and Knowledge Discovery in Databases: European Conference, ECML PKDD 2018, Dublin, Ireland, September 10–14, 2018, Proceedings, Part I 18*, pp. 3–17 (2019). Springer
- [32] van Hespen, K.M., Zwanenburg, J.J., Dankbaar, J.W., Geerlings, M.I., Hendrikse, J., Kuijf, H.J.: An anomaly detection approach to identify chronic brain infarcts on mri. *Scientific Reports* **11**(1), 7714 (2021)
- [33] Pinaya, W.H., Scarpazza, C., Garcia-Dias, R., Vieira, S., Baecker, L., F da Costa, P., Redolfi, A., Frisoni, G.B., Pievani, M., Calhoun, V.D., *et al.*: Using normative modelling to detect disease progression in mild cognitive impairment and alzheimer’s disease in a cross-sectional multi-cohort study. *Scientific reports* **11**(1), 1–13 (2021)
- [34] Chamberland, M., Genc, S., Tax, C.M., Shastin, D., Koller, K., Raven, E.P., Cunningham, A., Doherty, J., van den Bree, M.B., Parker, G.D., *et al.*: Detecting microstructural deviations in individuals with deep diffusion mri tractometry. *Nature computational science* **1**(9), 598–606 (2021)

- [35] Kim, D.-Y., Lee, S.J., Kim, E.-K., Kang, E., Heo, C.Y., Jeong, J.H., Myung, Y., Kim, I.A., Jang, B.-S.: Feasibility of anomaly score detected with deep learning in irradiated breast cancer patients with reconstruction. *npj Digital Medicine* **5**(1), 125 (2022)
- [36] Hendrycks, D., Gimpel, K.: A baseline for detecting misclassified and out-of-distribution examples in neural networks. *arXiv preprint arXiv:1610.02136* (2016)
- [37] Chen, J., Li, Y., Wu, X., Liang, Y., Jha, S.: Robust out-of-distribution detection for neural networks. *arXiv preprint arXiv:2003.09711* (2020)
- [38] Hsu, Y.-C., Shen, Y., Jin, H., Kira, Z.: Generalized ODIN: Detecting out-of-distribution image without learning from out-of-distribution data. In: *Proceedings of the IEEE/CVF Conference on Computer Vision and Pattern Recognition*, pp. 10951–10960 (2020)
- [39] Vyas, A., Jammalamadaka, N., Zhu, X., Das, D., Kaul, B., Willke, T.L.: Out-of-distribution detection using an ensemble of self supervised leave-out classifiers. In: *Proceedings of the European Conference on Computer Vision (ECCV)*, pp. 550–564 (2018)
- [40] Mohseni, S., Pitale, M., Yadawa, J., Wang, Z.: Self-supervised learning for generalizable out-of-distribution detection. In: *Proceedings of the AAAI Conference on Artificial Intelligence*, vol. 34, pp. 5216–5223 (2020)
- [41] DeVries, T., Taylor, G.W.: Learning confidence for out-of-distribution detection in neural networks. *arXiv preprint arXiv:1802.04865* (2018)
- [42] Zhang, C., Bengio, S., Hardt, M., Recht, B., Vinyals, O.: Understanding deep learning (still) requires rethinking generalization. *Communications of the ACM* **64**(3), 107–115 (2021)
- [43] Park, E., Lee, K., Han, T., Nam, H.S.: Automatic grading of stroke symptoms for rapid assessment using optimized machine learning and 4-limb kinematics: clinical validation study. *Journal of medical Internet research* **22**(9), 20641 (2020)
- [44] Kaku, A., Liu, K., Parnandi, A., Rajamohan, H.R., Venkataramanan, K., Venkatesan, A., Wirtanen, A., Pandit, N., Schambra, H., Fernandez-Granda, C.: Strokerehab: A benchmark dataset for sub-second action identification. *Advances in Neural Information Processing Systems* **35**, 1671–1684 (2022)
- [45] Parnandi, A., Kaku, A., Venkatesan, A., Pandit, N., Fokas, E., Yu, B., Kim, G., Nilsen, D., Fernandez-Granda, C., Schambra, H.: Data-driven quantitation of movement abnormality after stroke. *Bioengineering* **10**(6),

648 (2023)

- [46] Ambellan, F., Tack, A., Ehlke, M., Zachow, S.: Automated segmentation of knee bone and cartilage combining statistical shape knowledge and convolutional neural networks: Data from the osteoarthritis initiative. *Medical image analysis* **52**, 109–118 (2019)
- [47] Kohn, M.D., Sassoon, A.A., Fernando, N.D.: Classifications in brief: Kellgren-lawrence classification of osteoarthritis. *Clinical Orthopaedics and Related Research*® **474**, 1886–1893 (2016)
- [48] Eckstein, F., Wirth, W., Nevitt, M.C.: Recent advances in osteoarthritis imaging—the osteoarthritis initiative. *Nature Reviews Rheumatology* **8**(10), 622–630 (2012)
- [49] Hsu, H., Siwiec, R.M.: *Knee osteoarthritis* (2018)
- [50] Brody, L.T.: Knee osteoarthritis: Clinical connections to articular cartilage structure and function. *Physical Therapy in Sport* **16**(4), 301–316 (2015)
- [51] Geirhos, R., Jacobsen, J.-H., Michaelis, C., Zemel, R., Brendel, W., Bethge, M., Wichmann, F.A.: Shortcut learning in deep neural networks. *Nature Machine Intelligence* **2**(11), 665–673 (2020)
- [52] Guo, C., Pleiss, G., Sun, Y., Weinberger, K.Q.: On calibration of modern neural networks. In: *International Conference on Machine Learning*, pp. 1321–1330 (2017). PMLR
- [53] Liu, S., Kaku, A., Zhu, W., Leibovich, M., Mohan, S., Yu, B., Huang, H., Zanna, L., Razavian, N., Niles-Weed, J., *et al.*: Deep probability estimation. In: *International Conference on Machine Learning*, pp. 13746–13781 (2022). PMLR
- [54] Farha, Y.A., Gall, J.: Ms-tcn: Multi-stage temporal convolutional network for action segmentation. In: *Proceedings of the IEEE/CVF Conference on Computer Vision and Pattern Recognition*, pp. 3575–3584 (2019)
- [55] Ishikawa, Y., Kasai, S., Aoki, Y., Kataoka, H.: Alleviating over-segmentation errors by detecting action boundaries. In: *Proceedings of the IEEE/CVF Winter Conference on Applications of Computer Vision*, pp. 2322–2331 (2021)
- [56] Kingma, D.P., Ba, J.: Adam: A method for stochastic optimization. *arXiv preprint arXiv:1412.6980* (2014)

- [57] Feichtenhofer, C.: X3d: Expanding architectures for efficient video recognition. In: Proceedings of the IEEE/CVF Conference on Computer Vision and Pattern Recognition, pp. 203–213 (2020)
- [58] Kay, W., Carreira, J., Simonyan, K., Zhang, B., Hillier, C., Vijayanarasimhan, S., Viola, F., Green, T., Back, T., Natsev, P., et al.: The kinetics human action video dataset. arXiv preprint arXiv:1705.06950 (2017)
- [59] Perslev, M., Dam, E.B., Pai, A., Igel, C.: One network to segment them all: A general, lightweight system for accurate 3d medical image segmentation. In: Medical Image Computing and Computer Assisted Intervention–MICCAI 2019: 22nd International Conference, Shenzhen, China, October 13–17, 2019, Proceedings, Part II 22, pp. 30–38 (2019). Springer
- [60] Ronneberger, O., Fischer, P., Brox, T.: U-net: Convolutional networks for biomedical image segmentation. In: Medical Image Computing and Computer-Assisted Intervention–MICCAI 2015: 18th International Conference, Munich, Germany, October 5–9, 2015, Proceedings, Part III 18, pp. 234–241 (2015). Springer
- [61] Heusel, M., Ramsauer, H., Unterthiner, T., Nessler, B., Hochreiter, S.: GANs trained by a two time-scale update rule converge to a local nash equilibrium. *Advances in neural information processing systems* **30** (2017)

Appendix A Additional Dataset Information

Tables [A1](#) and [A2](#) provide a detailed description of the rehabilitation activities carried out by the subjects in the dataset used for quantification of stroke-induced impairment. Figure [A1](#) shows examples of the MRI scans used for quantification of knee-osteoarthritis severity.

Table A1 Description of the activities performed by the subjects in the dataset used for quantification of stroke-induced impairment (1/2).

Activity	Workspace	Target object(s)	Instructions
Face-wash	Sink with a small tub (32.3 x 24.1 x 2.5 cm ³) in it and two folded washcloths on either side of the countertop, 30 cm from edge closest to patient	Washcloths, faucet handle, and tub	Fill tub with water, dip washcloth on the right side into water, wring it, wiping each side of their face with wet washcloth, place it back on countertop. Use washcloth on the left side to dry face, place it back on countertop
Deodorant	Tabletop with deodorant placed at midline, 25 cm from edge closest to patient	Deodorant (solid twist-base)	Remove cap, twist base a few times, apply deodorant, replace cap, untwist the base, put deodorant on table
Combing	Tabletop with comb placed at midline, 25 cm from edge closest to patient	Comb	Pick up comb and comb both sides of head
Glasses	Tabletop with glasses placed at midline, 25 cm from edge closest to patient	Pair of glasses	Wear glasses, return hands to table, remove glasses and place on table
Feeding	Table top with a standard-size paper plate (21.6 cm diameter) placed at midline, 2 cm from edge, utensils placed 3 cm from edge, 5 cm from either side of plate, a baggie with a slice of bread placed 25 cm from edge, 23 cm left of midline, and a margarine packet placed 32 cm from edge, 17 cm right of midline	Paper plate, fork, knife, re-sealable sandwich baggie, slice of bread, single-serve margarine container	Remove bread from plastic bag and put it on plate, open margarine pack and spread it on bread, cut bread into four pieces, cut off and eat a small bite-sized piece

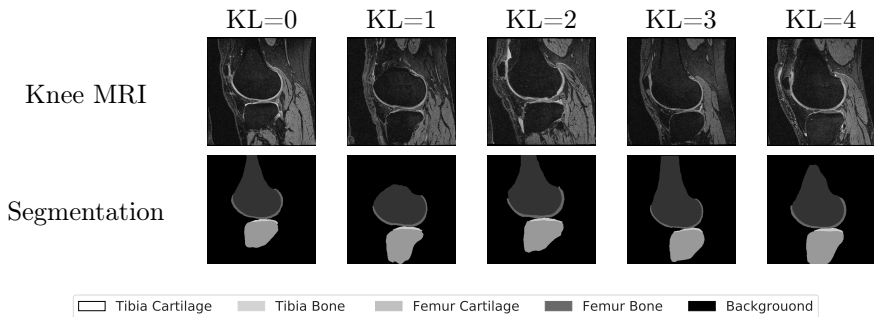
Appendix B Additional Results

B.1 Quantification of Impairment in Stroke Patients

Figures [B2](#), and [B3](#) show scatterplots of the FMA and COBRA scores for each rehabilitation activity. Tables [B3](#), [B4](#), and [B5](#) report the accuracy and precision of the AI models described in Section [4.2](#).

Table A2 Description of the activities performed by the subjects in the dataset used for quantification of stroke-induced impairment (2/2).

Activity	Workspace	Target object(s)	Instructions
Drinking	Tabletop with water bottle and paper cup 18 cm to the left and right of midline, 25 cm from edge closest to patient	Water bottle (12 oz), paper cup (4 oz)	Open water bottle, pour water into cup, take a sip of water, place cup on table, and replace cap on bottle
Brushing	Sink with toothpaste and toothbrush on either side of the countertop, 30 cm from edge closest to patient	Travel-sized toothpaste, toothbrush with built-up foam grip, faucet handle	Wet toothbrush, apply toothpaste to toothbrush, replace cap on toothpaste tube, brush teeth, rinse toothbrush and mouth, place toothbrush back on countertop
Table-top	Horizontal circular array (48.5 cm diameter) of 8 targets (5 cm diameter)	Toilet paper roll wrapped in self-adhesive wrap	Move the roll between the center and each outer target, resting between each motion and at the end
Shelf	Shelf with two levels (33 cm and 53 cm) with 3 targets on both levels (22.5 cm, 45 cm, and 67.5 cm away from the left-most edge)	Toilet paper roll wrapped in self-adhesive wrap	Move the roll between the center target and each target on the shelf, resting between each motion and at the end

**Fig. A1** Knee MRI images for subjects with different Kellgren-Lawrence (KL) grades (top) and corresponding segmentation annotations (bottom) indicating the tissue in each pixel.

In Figure 5 we show that object color is a confounding factor, which can spuriously reduce model confidence and therefore distort the COBRA score. To complement this observation, we analyzed the impact of varying video resolution on the COBRA score. We blurred half of the videos (chosen at random), reducing their resolution by a factor of 16 along each axis and then restoring them to their original dimensions. Figure B4 shows the results of applying the COBRA score to a dataset containing the blurred and non-blurred videos. Blurring acts as a confounding factor, producing a spurious decrease in model confidence independent of impairment, which reduces the correlation

Table B3 Performance of the AI models used to compute the COBRA score for quantification of stroke-induced impairment from wearable-sensor data on held-out healthy subjects. 95% CIs are shown in brackets.

Activity	Motion-based Accuracy	Motion-based Precision	Overall Accuracy	Overall Precision
All	0.734 [0.726,0.747]	0.781 [0.773,0.791]	0.755 [0.747,0.761]	0.719 [0.712,0.726]
Brushing	0.588 [0.574,0.602]	0.613 [0.598,0.625]	0.661 [0.652,0.672]	0.616 [0.605,0.624]
Combing	0.815 [0.803,0.826]	0.804 [0.794,0.816]	0.763 [0.750,0.777]	0.735 [0.725,0.746]
Deodorant	0.692 [0.681,0.702]	0.693 [0.682,0.705]	0.718 [0.708,0.726]	0.682 [0.674,0.691]
Drinking	0.696 [0.686,0.708]	0.740 [0.729,0.748]	0.743 [0.736,0.751]	0.710 [0.703,0.716]
Face-wash	0.605 [0.591,0.616]	0.628 [0.618,0.638]	0.585 [0.572,0.593]	0.569 [0.561,0.576]
Feeding	0.623 [0.608,0.642]	0.643 [0.625,0.662]	0.676 [0.662,0.688]	0.653 [0.642,0.665]
Glasses	0.781 [0.773,0.790]	0.768 [0.759,0.775]	0.699 [0.690,0.709]	0.686 [0.678,0.693]
Shelf	0.831 [0.822,0.838]	0.927 [0.922,0.932]	0.835 [0.827,0.843]	0.773 [0.765,0.779]
Table-top	0.807 [0.801,0.813]	0.874 [0.868,0.879]	0.746 [0.736,0.759]	0.716 [0.710,0.723]

Table B4 Performance of the AI models used to compute the COBRA score for quantification of stroke-induced impairment from wearable-sensor data on subjects with different levels of impairment. Performance degrades as the impairment level increases. 95% CIs are shown in brackets.

Impairment Level	Motion-based Accuracy	Motion-based Precision	Overall Accuracy	Overall Precision
Healthy	0.747 [0.738,0.757]	0.773 [0.763,0.783]	0.753 [0.743,0.760]	0.725 [0.716,0.732]
Mild	0.707 [0.696,0.716]	0.689 [0.678,0.697]	0.674 [0.666,0.681]	0.669 [0.661,0.676]
Moderate	0.541 [0.532,0.551]	0.536 [0.535,0.551]	0.545 [0.539,0.552]	0.570 [0.562,0.578]
Severe	0.354 [0.342,0.367]	0.333 [0.321,0.346]	0.373 [0.364,0.383]	0.395 [0.386,0.405]

between FMA and the COBRA score. This can be corrected by stratifying the videos, separating them according to whether they are blurred or not.

B.2 Quantification of Knee-Osteoarthritis Severity

Table B7 reports the pixel-wise accuracy and precision of the AI model described in Section 4.3.

Table B5 Performance of the AI models used to compute the COBRA score for quantification of stroke-induced impairment from video data on held-out healthy subjects. 95% CIs are shown in brackets.

Activity	Motion-based Accuracy	Motion-based Precision	Overall Accuracy	Overall Precision
All	0.732 [0.720,0.740]	0.654 [0.643,0.663]	0.608 [0.597,0.616]	0.661 [0.650,0.672]
Brushing	0.781 [0.766,0.795]	0.709 [0.692,0.720]	0.611 [0.599,0.622]	0.670 [0.656,0.680]
Combing	0.714 [0.706,0.724]	0.817 [0.803,0.831]	0.547 [0.540,0.556]	0.631 [0.623,0.639]
Deodorant	0.629 [0.618,0.643]	0.512 [0.497,0.529]	0.443 [0.435,0.453]	0.576 [0.562,0.590]
Drinking	0.619 [0.605,0.633]	0.542 [0.527,0.557]	0.493 [0.482,0.502]	0.539 [0.526,0.551]
Face-wash	0.648 [0.635,0.661]	0.645 [0.633,0.660]	0.469 [0.461,0.478]	0.560 [0.551,0.573]
Feeding	0.524 [0.502,0.541]	0.421 [0.399,0.446]	0.467 [0.454,0.478]	0.494 [0.477,0.508]
Glasses	0.708 [0.699,0.715]	0.673 [0.399,0.446]	0.513 [0.454,0.478]	0.667 [0.477,0.508]
Shelf	0.717 [0.709,0.726]	0.633 [0.624,0.642]	0.556 [0.506,0.519]	0.612 [0.568,0.655]
Table-top	0.768 [0.760,0.777]	0.693 [0.683,0.702]	0.614 [0.605,0.623]	0.620 [0.603,0.637]

Table B6 Performance of the AI models used to compute the COBRA score for quantification of stroke-induced impairment from video data on subjects with different levels of impairment. Performance degrades as the impairment level increases. 95% CIs are shown in brackets.

Impairment Level	Motion-based Accuracy	Motion-based Precision	Overall Accuracy	Overall Precision
Healthy	0.732 [0.722,0.742]	0.654 [0.643,0.664]	0.608 [0.599,0.618]	0.662 [0.652,0.672]
Mild	0.615 [0.605,0.627]	0.501 [0.492,0.512]	0.505 [0.497,0.513]	0.551 [0.542,0.561]
Moderate	0.555 [0.546,0.566]	0.421 [0.411,0.432]	0.441 [0.433,0.448]	0.496 [0.487,0.505]
Severe	0.425 [0.410,0.439]	0.348 [0.338,0.356]	0.352 [0.341,0.362]	0.339 [0.330,0.348]

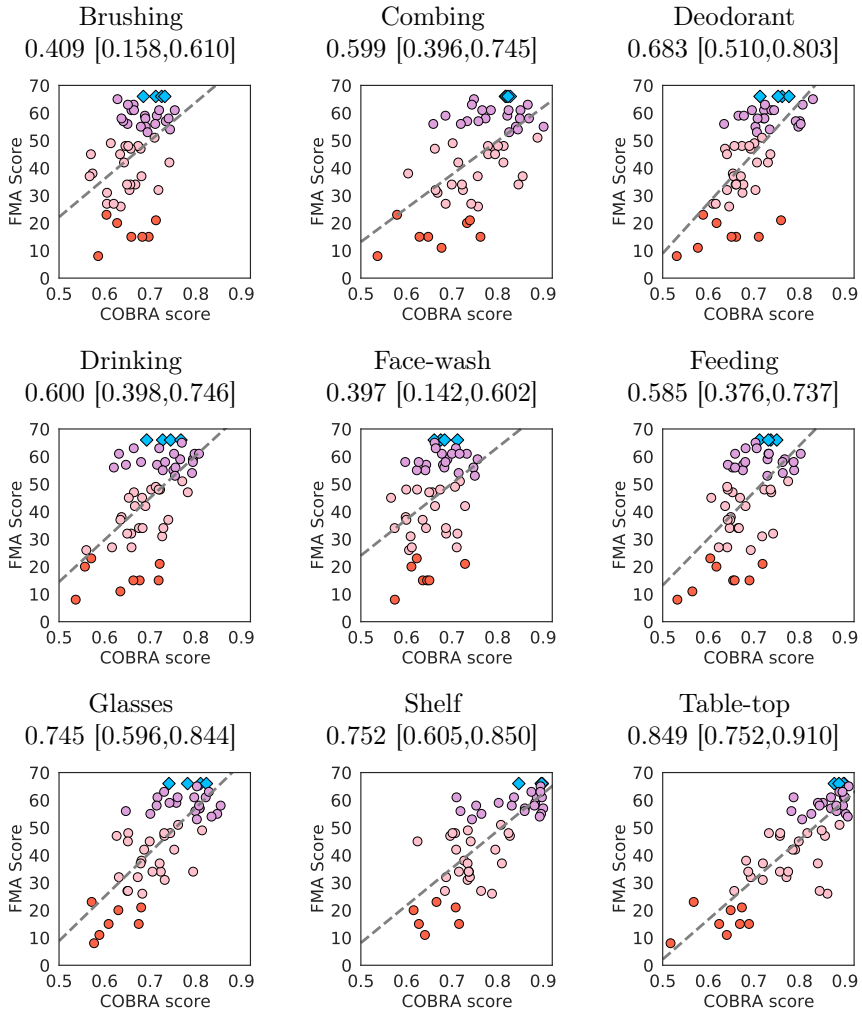


Fig. B2 Correlation between wearable-sensor COBRA score and clinical assessment for individual rehabilitation activities. Scatterplots of the Fugl-Meyer assessment (FMA) score, based on in-person examination by an expert, and the proposed data-driven COBRA score computed from wearable-sensor data for individual rehabilitation activities. The correlation coefficient ρ is highest for simpler more structured activities such as Glasses, Shelf and Table-top.

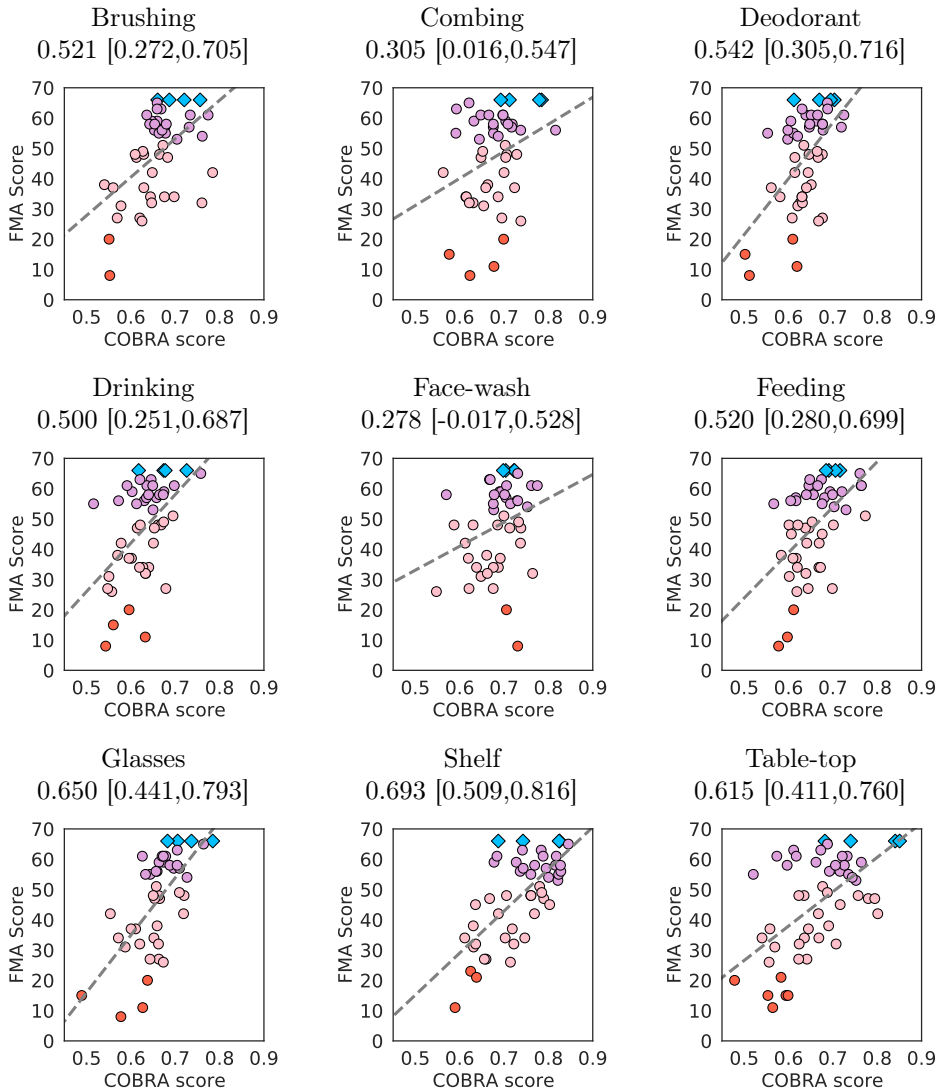


Fig. B3 Correlation between video COBRA score and clinical assessment for individual rehabilitation activities. Scatterplots of the Fugl-Meyer assessment (FMA) score, based on in-person examination by an expert, and the proposed data-driven COBRA score computed from video data for individual rehabilitation activities. The correlation coefficient ρ is highest for simpler more structured activities such as Glasses, Shelf and Table-top.

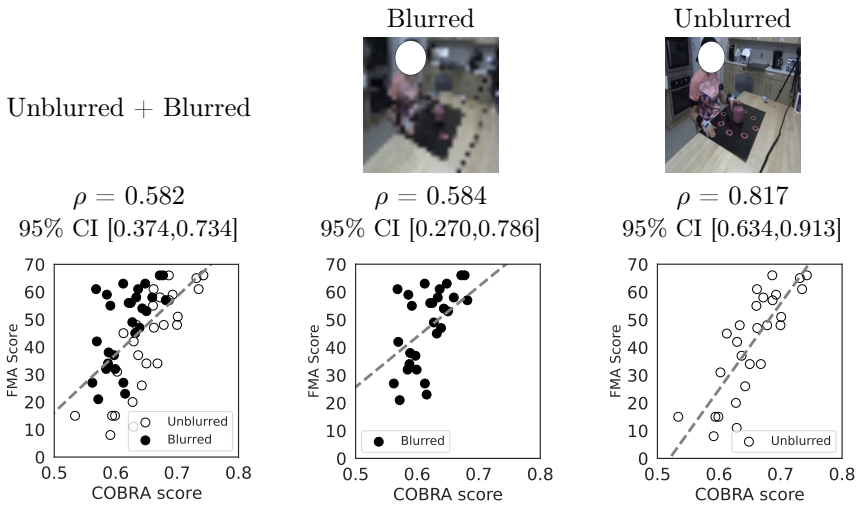


Fig. B4 Video quality as a confounding factor for the video-based COBRA score. Vision models are sensitive to video quality. One example is the blurring effect. The bottom left scatterplot shows the COBRA score computed from blurred and non-blurred videos, as well as the corresponding Fugl-Meyer assessment (FMA) score. Blurring decreases model confidence, systematically decreasing the COBRA score. The bottom middle and right scatterplots show that stratifying the videos according to their quality corrects for the confounding factor, improving the correlation coefficient ρ between the COBRA and FMA scores.

Table B7 Pixel-wise performance of the AI models used to compute the COBRA score for quantification of knee-osteoarthritis severity from MRI scans on held-out healthy subjects. 95% CIs are shown in brackets.

Group	Accuracy	Precision
KL = 0 (Healthy)	0.995 [0.993,0.997]	0.922 [0.878,0.952]
KL = 1 (Doubtful)	0.994 [0.992,0.996]	0.922 [0.890,0.956]
KL = 2 (Minimal)	0.994 [0.990,0.996]	0.907 [0.852,0.945]
KL = 3 (Moderate)	0.992 [0.983,0.996]	0.885 [0.816,0.931]
KL = 4 (Severe)	0.991 [0.979,0.995]	0.851 [0.721,0.917]

Appendix C Distance-based Anomaly Quantification

In this section we present an alternative method for anomaly detection and quantification that utilizes an AI model trained only on healthy patients. The method is based on the Fréchet Inception Distance (FID) [61] to quantify the deviation between a subject and a healthy population. FID is a metric designed to evaluate the similarity between two sets of feature representations extracted by a deep neural network. It has been applied to image generation [61], where the goal is to determine whether generated images are close to real images or not.

We propose to leverage FID to compare a potentially impaired subject to a healthy reference population using the same model features as in the COBRA framework. First, the data associated with all individuals is fed into a deep neural network, trained to perform a task relevant to the impairment or disease of interest. Then, the features extracted by the neural network are compared via FID to determine to what extent the subject deviates from the population.

Let x_1, x_2, \dots, x_n be the features associated with the healthy reference subjects, and y_1, y_2, \dots, y_m the feature representations of the potentially-impaired subject. The sample mean and covariance matrices of these features are denoted by μ_x, μ_y and Σ_x, Σ_y , respectively. The FID between the healthy population and the impaired subject is

$$\text{FID}(x, y) = \|\mu_x - \mu_y\|_2^2 + \text{Trace}(\Sigma_x + \Sigma_y - 2(\Sigma_x \Sigma_y)^{1/2}), \quad (\text{C1})$$

where $\text{Trace}(\cdot)$ denotes the trace operator and $\|\cdot\|_2$ is the ℓ_2 norm. The lower the FID between the two sets of features, the more similar they are.

As a proof of concept, we apply FID to quantification of stroke-induced impairment using the sensor dataset described in Section 2.1. We apply the model described in Section 4.2.1, trained on the training cohort of healthy patients. The features used to compute the FID are extracted from the penultimate layer of the model. Two held-out healthy subjects from the test cohort were randomly chosen to be the reference healthy population. The FID of the remaining subjects of the test cohort was computed with respect to this population.

Table C8 shows the correlation coefficient of the FID with respect to the reference healthy subjects and the Fugl-Meyer assessment (FMA) for different rehabilitation activities. The magnitude of the correlation is higher when motion primitives are utilized to compute the FID, and for more structured activities. The metrics are not as correlated as the COBRA score and FMA (see Figure B2), but these results suggest that there may be multiple ways of exploiting features extracted from AI models to perform anomaly detection and quantification.

Table C8 Correlation between Fréchet Inception Distance (FID) and clinical assessment. Correlation coefficient between the FID (with respect to a reference healthy population) computed from wearable-sensor data and the Fugl-Meyer assessment for different rehabilitation activities. The metrics are more correlated when motion primitives are utilized to compute the FID, and for more structured activities. 95% CIs are shown in brackets.

Activity	Non-motion	Motion	All primitives
All	-0.359 [-0.461,-0.025]	-0.715 [-0.780,-0.647]	-0.650 [-0.719,-0.577]
Brushing	-0.041 [-0.249,0.225]	-0.176 [-0.426,0.001]	-0.139 [-0.287,0.078]
Combing	-0.329 [-0.434,-0.140]	-0.427 [-0.703,-0.025]	-0.313 [-0.469,-0.087]
Deodorant	-0.280 [-0.500,-0.081]	-0.693 [-0.793,-0.402]	-0.617 [-0.712,-0.493]
Drinking	-0.243 [-0.433,-0.032]	-0.352 [-0.477,-0.183]	-0.436 [-0.563,-0.277]
Face-wash	-0.246 [-0.433,-0.004]	-0.255 [-0.464,0.025]	-0.347 [-0.491,-0.217]
Feeding	-0.429 [-0.625,-0.230]	-0.396 [-0.561,-0.160]	-0.523 [-0.675,-0.329]
Glasses	-0.510 [-0.619,-0.270]	-0.688 [-0.760,-0.599]	-0.718 [-0.795,-0.624]
Shelf	-0.254 [-0.461,-0.034]	-0.684 [-0.760,-0.580]	-0.597 [-0.699,-0.439]
Table-top	-0.533 [-0.640,-0.418]	-0.693 [-0.758,-0.605]	-0.609 [-0.694,-0.492]